Uniformly valid asymptotic flow analysis in curved channels

M. Zagzoule,[1,a)] P. Cathalifaud,[1,b)] J. Cousteix,[2,c)] and J. Mauss[1,d)]
[1]*Université de Toulouse, INPT, UPS, CNRS, IMFT, F-31400 Toulouse, France*
[2]*ONERA - The French Aerospace Lab, ISAE, F-31055 Toulouse, France*

The laminar incompressible flow in a two-dimensional curved channel having at its upstream and downstream extremities two tangent straight channels is considered. A global interactive boundary layer (GIBL) model is developed using the approach of *the successive complementary expansions method* (SCEM) which is based on generalized asymptotic expansions leading to a uniformly valid approximation. The GIBL model is valid when the non dimensional number $\mu = \delta R_e^{\frac{1}{3}}$ is O(*1*) and gives predictions in agreement with numerical Navier-Stokes solutions for Reynolds numbers R_e ranging from 1 to 10^4 and for constant curvatures $\delta = \frac{H}{R_c}$ ranging from 0.1 to 1, where H is the channel width and R_c the curvature radius. The asymptotic analysis shows that μ, which is the ratio between the curvature and the thickness of the boundary layer of any perturbation to the Poiseuille flow, is a key parameter upon which depends the accuracy of the GIBL model. The upstream influence length is found asymptotically and numerically to be $O(R_e^{\frac{1}{7}})$.

I. INTRODUCTION

Curvature is involved in many flow situations, whether it flows in man made devices or natural ones as physiological flows for instance. To characterize, the flow modifications induced by curvature many studies have been published since the pioneering work by Dean[1,2] who treated the case of small curvature. Many reviews can be consulted among which those of Berger *et al.*,[3] Pedley,[4] Ito,[5] or Ward-Smith.[6,7] The problems addressed previously were those associated with upstream (and entry) effects, downstream effects, and fully established flow characteristics. The methods used to get local or global insight ranged from asymptotic, analytic, or numerical simulations, mostly for curved pipes where secondary flows were essentially concerned.

Very rare studies dealt with the 2D channel flow where no azimuthal secondary flow occurs (Hurd and Peters[8] and Snyder and Lovely[9]). This simpler situation can provide useful informations, on one hand about the effects of the curvature compared to an otherwise straight channel and on the other hand compared to a 3D curved pipe case by discriminating the plane aspects from the complex interaction with the azimuthal secondary flow. Moreover, the channel curved configuration still keeps in its mathematical formulation, asymptotic and physical analysis not to mention its numerical resolution, some interesting features which must be clarified before tackling the more complex curved pipe case.

In general, modern asymptotic studies of the flow field structure, internal or external, extensively used the triple deck theory.[10,11] This method based on regular asymptotic developments of the Poincaré type involves complex asymptotic matchings between different zones because the underlying assumptions lead to a strong coupling between the two boundary layers in the case of

[a)]Electronic mail: zagzoule@imft.fr.
[b)]Electronic mail: catalifo@imft.fr.
[c)]Electronic mail: Jean.Cousteix@onecert.fr.
[d)]Electronic mail: mauss@cict.fr.

channel flows. A different approach termed SCEM, (successive complementary expansions method), in which one assumes *a priori* a uniformly valid approximation (UVA) based on generalized expansions, is adopted in the present work. This method was developed by Cousteix and Mauss[12,13] and leads to an asymptotic reduced model called *global interactive boundary layer (GIBL)*. This method avoids the complex and subtle process of constructing formally the asymptotic matching between the boundary layers and core flow to build the solution of the flow field in the whole domain.

We consider in the following, a two-dimensional laminar flow of an incompressible Newtonian fluid in a uniformly curved channel at high Reynolds number R_e. The fact that the Reynolds number R_e is large makes it possible to consider an asymptotic analysis, in order to obtain a simpler model than the Navier-Stokes (NS) equations.

In Sec. II, we start by writing the Cauchy equations in a curvilinear coordinate system (Eqs. (A1)–(A3)). For a channel, where the curvature is uniform, $K = \delta$, K being defined as the ratio of the channel width H to the curvature radius R_c, i.e., $K = H/R_c$, we deal with the fully developed flow case where the velocity field is independent of X and obtain an analytical expression for the axial velocity irrespective of the order of magnitude of K. An interesting feature is the appearance of KY in the viscous term as a variable added viscosity. For this established flow, we derive a simple expression for the fully established velocity profile in the case of K being small (see Eq. (11)).

In Sec. IV, we apply the SCEM to obtain the core flow behavior. Upon the assumption of a small curvature parameter $(K \prec\prec 1)$, we extract a reduced NS valid up to O(K) (Eqs. (16)–(18)) to which the SCEM is applied to obtain the core flow behaviour. The resulting linear Euler equations couples the known upstream basic Poiseuille flow with the perturbations induced by the curvature (Sec. IV C). This is followed in Sec. IV D by a close analysis of the order of magnitude of the core pressure as it impacts on the boundary layer. It is found there that the correction or additional term to the longitudinal pressure gradient in the boundary layer is negligible relative to the one that satisfies the linear Euler model in the core flow and we end up with the key result for the pressure gradient in the whole domain being

$$\frac{\partial P}{\partial X} = \frac{\mathrm{d}p_0}{\mathrm{d}X} + \delta\left(\frac{\partial p_1}{\partial X} + \mathrm{O}(\varepsilon^3)\right),$$

where in the right-hand side the first term represents the basic Poiseuille pressure gradient, the second the core pressure gradient induced by the perturbation, and the third the order of neglected correction gradient in the boundary layer. In Sec. V, after noticing that the boundary layer velocity corrections vanish in the core flow, the GIBL model consisting of the Eqs. (37) and (38) associated with the core flow Eqs. (31) and (32) gives an *approximation valid in the whole channel*.

Unlike the triple deck boundary layer's equations where the transverse Y variable is local, the GIBL model deals with a global Y that varies from wall to wall. Moreover, the Eqs. (37) and (38) "naturally" reduce to the linear Euler equations in the core. In fact, this limiting behaviour is used to couple the core and the boundary layer flows, through the condition of equality of the transverse velocities at the median line (Eq. (39)) as well as the pressure gradient expression mentioned previously. The originality of the method presented in this paper is that it takes into account not only the perturbed zones in between Poiseuillian established ones but also the transition between the curved entry flow zone induced by the curvature discontinuity and the curved established part. This is done without having to build first the longitudinal asymptotic matching between these two curved regions as triple deck approach has to do. The GIBL version of the present work is the result of two asymptotic levels: first a regular asymptotic $O(\delta)$ model of the Dean type is built, upon which, in a second step, a high Reynolds singular asymptotic approach is applied. In doing so, it captures the whole field flow effects induced by the curvature of the channel regardless of them being of the entry type or established ones while considering the curvature as a perturbation.

The validity of the GIBL model is tested in Sec. VI against full Navier-Stokes numerical resolution. The predictive capacity of this GIBL model is more than satisfactory as shown through many examples.

II. FORMULATION

A. General equations

If the characteristic length, velocity, and pressure are chosen, respectively, as H, U^*, and ρU^{*2}, the steady dimensionless equations can be written

$$(\vec{V}\cdot\vec{\nabla})\vec{V} = -\vec{\nabla}\Pi + \frac{1}{R_e}\Delta\vec{V}, \quad \mathrm{div}\vec{V} = 0, \tag{1}$$

where $\vec{V}$ is the velocity, Π the pressure, and R_e the Reynolds number. The Reynolds number is given by

$$R_e = \frac{\rho\, U^* H}{\mu^*}, \tag{2}$$

where μ^* is the viscosity.

A typical geometrical configuration considered in this paper consists of a 2D bend connected to two tangent straight channels at its extremities (see Figure 1). For a channel defined, in the cartesian system Oxy, by the boundaries $y = \pm\frac{1}{2}$ when $x<0$ and for a flow rate of $1/6$, the basic plane Poiseuille flow can be written,

$$u_0(y) = \frac{1}{4} - y^2, \quad v_0 = 0, \quad \frac{\mathrm{d}p_0}{\mathrm{d}x} = -\frac{2}{R_e}. \tag{3}$$

Let the bend starts at $x=0$ and consider a line such as,

$$\mathcal{H}(x,y) = 0, \tag{4}$$

If X is the measure of distance of the point M_0 along $\mathcal{H}=0$, then the lines $X=$ constant are the normal to $\mathcal{H}=0$. For the curves $Y=$ constant, we take the parallel lines to $\mathcal{H}=0$, each of which intersects the normal lines at constant distance from this median line. So, quite generally, X and Y are, respectively, distances along the line $\mathcal{H}=0$ and perpendicular to the line $\mathcal{H}=0$. It is the median line if the upper (or inner) and lower (or external) walls are, respectively, given by $Y=\pm\frac{1}{2}$.

For a point M with general coordinates X and Y, we can write $\overrightarrow{OM} = \overrightarrow{OM_0} + Y\vec{n}$, where $\vec{n}$ is the unit normal vector. Then,

$$\overrightarrow{\mathrm{d}M} = \mathrm{d}X(1+KY)\vec{\tau} + \mathrm{d}Y\vec{n}, \tag{5}$$

where $\vec{\tau}$ is the unit vector tangent at M_0 to the median line in such a way that the orientation of $(\vec{\tau},\vec{n})$ is positive or right-handed; $K(X)$ is the algebraic curvature of this line. Thus, $K<0$ in the case of Figure 1.

Let U and V denote the velocity components parallel and perpendicular to the line $\mathcal{H}=0$, then, since $\vec{V} = U\vec{\tau} + V\vec{n}$, the full equations of motion written in generalized coordinates are given

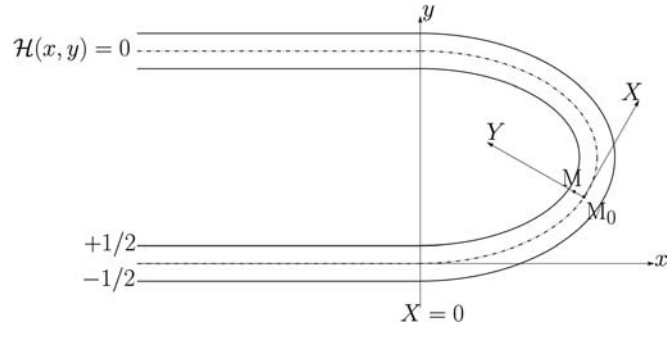

FIG. 1. The typical geometrical configuration considered: 2D bend connected to 2 straight channels at its extremities.

in the Appendix A. We choose this coordinates system because of the possibility to handle problems with non-constant curvature.

These equations must be solved with the following boundary conditions:

$$U = V = 0 \quad \text{for} \quad Y = \pm\frac{1}{2}. \tag{6}$$

B. Fully established flow

For a channel where the curvature is uniform, $K = \delta$, the established velocity field $U = U_0$ is independent of X. In the stationary case, $G = -\frac{\partial P}{\partial X}$ is a constant and U_0 is solution of the equation,

$$(1+\delta Y)\frac{\mathrm{d}^2U_0}{\mathrm{d}Y^2} + \delta\frac{\mathrm{d}U_0}{\mathrm{d}Y} - \frac{\delta^2}{1+\delta Y}U_0 = -GR_e, \tag{7}$$

with $U_0 = 0$ for $Y = \pm\frac{1}{2}$.

The exact solution can readily be obtained and is given by

$$U_0(Y) = \frac{1}{64}GR_e\frac{f(\delta,Y)}{\delta^2(1+\delta Y)}, \tag{8}$$

where

$$\begin{aligned} f(\delta,Y) = &\left[\delta^3(1-4Y^2) + 8\delta^2Y(2Y-1) + 4\delta(-4Y^2+8Y-3) + 16(1-2Y)\right]\ln\left(\frac{2-\delta}{2\delta}\right) \\ &+ \left[-\delta^3(1-4Y^2) + 8\delta^2Y(2Y+1) + 4\delta(4Y^2+8Y+3) + 16(1+2Y)\right]\ln\left(\frac{2+\delta}{2\delta}\right) \\ &- 32\left(2\delta Y + \delta^2Y^2 + 1\right)\ln\left(\frac{1+\delta Y}{\delta}\right). \end{aligned}$$

Unlike pipe flows, the fully developed 2D flow for a small constant curvature δ, $U_0(Y)$, is solution of the following simple equation:

$$\frac{\mathrm{d}}{\mathrm{d}Y}\left[(1+\delta Y)\frac{\mathrm{d}U_0}{\mathrm{d}Y}\right] = -G_1R_e, \tag{9}$$

whose analytical solution is

$$U_0(Y) = -\frac{G_1R_e}{\delta}\left[-Y - \frac{\ln\left[\frac{-(\delta-2)(\delta+2)}{4\delta^2}\right]}{2\ln\left[\frac{-(\delta+2)}{\delta-2}\right]} + \ln\left[\frac{-(\delta+2)}{\delta-2}\right]\ln\left[\frac{1+\delta Y}{\delta}\right]\right]. \tag{10}$$

At the order δ, the solution of the Eq. (9) is,

$$U_0 = \frac{G_1R_e}{2}\left(\frac{1}{4} - Y^2\right)\left(1 - \frac{2\delta}{3}Y\right). \tag{11}$$

This simple result shows that the fully developed axial velocity profile is skewed slightly towards the inside of the channel bend. This is quite different from the pipe flow case where, due to azimuthal secondary flow, there is, for large R_e, a strong skew outwards of the pipe. This slight skewing towards the internal side leads to a maximum of the velocity approximately located beside the median line at $Y_{\max} \approx -\frac{\delta}{12}$.

Moreover, since the flow rate is $1/6$, the pressure gradient in Eq. (11) is exactly $GR_e = 2$ as if the curvature was zero. Thus, the axial velocity profile is written,

$$U_0 = \left(\frac{1}{4} - Y^2\right)\left(1 - \frac{2\delta}{3}Y\right). \tag{12}$$

The skin friction coefficient C_f is given by,

$$C_f = \mp \frac{2}{R_e}\frac{\mathrm{d}U_0}{\mathrm{d}Y}\bigg|_{Y=\pm\frac{1}{2}}. \tag{13}$$

As with Eq. (12), we have $\frac{\mathrm{d}U_0}{\mathrm{d}Y}\big|_{Y=\pm\frac{1}{2}} = \mp 1 + \frac{\delta}{3}$, thus the final result is,

$$C_f \frac{R_e}{2} = 1 \mp \frac{\delta}{3}. \tag{14}$$

If we note C_f^{curved} and C_f^{straight} the skin friction for the curved and straight channels, respectively, we have $\frac{C_f^{\text{curved}} - C_f^{\text{straight}}}{C_f^{\text{straight}}} = \mp\frac{\delta}{3}$ thus the shear stress in the curved internal wall will exceed the Poiseuille case by 11% for $\delta = 1/3$ or 6.6% for $\delta = 0.2$, for example.

III. OVERALL PRESENTATION OF THE METHOD

The main objective of this work is to show that, subject to some order constraints, a UVA, (U,V,P), can be computed and is relatively accurate. Along the asymptotic process, it is found that this UVA verifies boundary layer like equations valid in the entire flow field and that the pressure gradient of the core flow is asymptotically a good UVA of the pressure gradient. Thus, the core longitudinal pressure gradient deduced from the linearised Euler equations is sufficient to drive the entire axial flow.

This process can be viewed as a *composite asymptotic expansion* and have the main advantage of avoiding formal matching of a separate boundary-layer solution to a core flow (though the boundary layers must still be resolved numerically when solving for the axial flow). This process has an original approach which is the *inverse of the standard ones* since it *starts with a UVA* and seeks afterwards what is its behaviour in the core.

In practice, the method goes through 4 main steps

(1) The formal writting of the uniformaly valid approximation (U,V,P) as an asymptotic expansion. In this step, we use a SCEM;
(2) The analysis of the pressure magnitude orders. This step ends up finding that the core pressure is a UVA, i.e., $(U,V,P) = (U,V,P_1)$, where P_1 stands for the pressure in the core flow;
(3) The formulation of the equations of the UVA. This step ends up finding that (U,V,P_1) is solution of boundary layer-like equations;
(4) The use of a long wave approximation to obtain a simplified expression for the pressure P_1. This step is not necessary.

The Sec. IV will be devoted to the first and second steps and the Sec. V to the third and fourth steps.

The main physical ideas behind the second and third steps are

(a) that the pressure variations in the core of the flow can be calculated by solution of the linearized Euler equations.
(b) that these pressure variations are transmitted through a negotiated strong coupling and with little variation across the boundary layers.
(c) that the boundary layer approximation (neglect of $R_e^{-1}\frac{\partial^2 U}{\partial X^2}$) can be applied to the entire flow and not just the boundary layers.

IV. ASYMPTOTIC ANALYSIS

Notice that in this paper, we use A = O(B) to mean that A is at most the same order as B and possibly less.

A. The equations

The objective that we set now is to find a simpler model than the Navier-Stokes equations using the least possible restrictive asymptotic assumptions. For this purpose, it is assumed that the curvature K and its variation in X are small.

We describe the channel variable curvature for $X > 0$ by

$$K = \delta k(X), \tag{15}$$

where δ is a small positive parameter.

Since we are considering high Reynolds number, the basic flow is dominated by its longitudinal component, therefore, all the terms are small except U, $\frac{\partial U}{\partial Y}$, $\frac{\partial^2 U}{\partial Y^2}$, and $\frac{\partial P}{\partial X}$ which are of order 1.

Then, to order δ included, continuity equation and Navier-Stokes equations can be written in the stationary case,

$$\frac{\partial U}{\partial X} + \frac{\partial V}{\partial Y} = 0, \tag{16}$$

$$L_\varepsilon U = U\frac{\partial U}{\partial X} + V\frac{\partial U}{\partial Y} + \frac{\partial P}{\partial X} - \frac{1}{R_e}\left(\frac{\partial^2 U}{\partial X^2} + \frac{\partial}{\partial Y}\left[(1+KY)\frac{\partial U}{\partial Y}\right]\right) = 0, \tag{17}$$

$$L_\varepsilon V = U\frac{\partial V}{\partial X} - KU^2 + \frac{\partial P}{\partial Y} - \frac{1}{R_e}\left(\frac{\partial^2 V}{\partial X^2} + \frac{\partial^2 V}{\partial Y^2}\right) = 0. \tag{18}$$

Note that at this O(δ) approximation, the curvature is appearing only twice: in the viscous term of the longitudinal momentum equation as a *variable viscosity* and in the KU^2 centrifugal/inertial part of the transversal momentum equation. The streamline curvature creates a radial pressure gradient which is very important for upstream influence. To simplify the notation, the unknowns are still denoted (U,V,P), even if now it is a *uniformly valid approximation*.

B. Using the SCEM

The fact that the Reynolds number is high is clearly important when perturbation occurs. In our stationary case, this perturbation can be for instance a change in the geometry of the walls or a variation in the curvature. Thus, Navier-Stokes equations *for the perturbation* reduce to the first order equations and we are faced with a singular perturbation problem. In order to satisfy the no-slip condition at the walls, we must define boundary layers. To achieve this, a convenient mathematical approach is the SCEM.

We seek a solution in the form,

$$U = u_0 + \delta u, \quad V = \delta v, \tag{19}$$

where $u_0(Y) = \frac{1}{4} - Y^2$. Therefore, in the core flow, the approximations in terms of generalized expansions can be written,

$$\begin{aligned} U_1 &= u_0(Y) + \delta u_1(X,Y,\delta), \\ V_1 &= \delta v_1(X,Y,\delta), \\ P_1 &= p_0(X) + \delta p_1(X,Y,\delta), \end{aligned} \tag{20}$$

where $p_0(X) = -\frac{2X}{R_e}$. Note that the dependence on the Reynolds number is implicit. If we consider the flow near a wall, say the lower wall to fix ideas, since the Reynolds number is large, a boundary layer of yet unknown thickness ε will develop. In the neighbourhood of this wall, the boundary layer variable is,

$$\eta = \frac{\frac{1}{2} + Y}{\varepsilon}. \tag{21}$$

According to the SCEM, a UVA is obtained by complementing the core approximation Eq. (20) with boundary layer terms,

$$U = u_0(Y) + \delta(u_1(X,Y,\delta) + U_{BL}(X,\eta,\delta)), \tag{22}$$

$$V = \delta(v_1(X,Y,\delta) + \varepsilon V_{BL}(X,\eta,\delta)), \tag{23}$$

$$P = p_0(X) + \delta(p_1(X,Y,\delta) + \Delta(\varepsilon)P_{BL}(X,\eta,\delta)). \tag{24}$$

The terms U_{BL}, V_{BL}, and P_{BL} being O(1), are correcting terms, respectively, to u_1, v_1, and p_1 in the boundary layer such that $\lim_{\eta\to\infty} U_{BL} = 0$, $\lim_{\eta\to\infty} V_{BL} = 0$, and $\lim_{\eta\to\infty} P_{BL} = 0$.

Again, the quantities (U,V,P) do not represent the exact solution but only a uniformly valid approximation for the core and the lower boundary layer. The form of V is imposed by the continuity equation. We can evaluate the boundary layer thickness ε in a O(1) neighbourhood of the perturbation. Actually, in the longitudinal equation, in order to have the same order for the inertial and viscous terms and since $u_0 = \mathrm{O}(\varepsilon)$ in the boundary layer,

$$\varepsilon = R_e^{-\frac{1}{3}}. \tag{25}$$

To satisfy the hypothesis of Eq. (22), i.e., $\delta u = \mathrm{O}(\varepsilon)$ as a limit case, necessarily

$$\delta = \mathrm{O}(\varepsilon) \tag{26}$$

which means that

$$\delta = \mathrm{O}\left(R_e^{-\frac{1}{3}}\right). \tag{27}$$

According to Eq. (27), a characteristic number in this 2D curved channel is

$$\mu = \delta R_e^{\frac{1}{3}} \tag{28}$$

μ can be seen as the ratio between the curvature δ and the boundary layer thickness ε around the discontinuities, and from Eqs. (25) and (27) $\mu = \mathrm{O}(1)$.

Thus, the first significant perturbation is obtained when ε and δ are of the same order, and permits U to be negative in the boundary layer. This challenging case is when μ is of strict order 1, $\mu = 1$. A special attention will thus be paid to this challenging case in the tested configurations on Sec. VI. It should be noted that although we have an analytical solution for the curved established flow valid for all δ, the fact that $\mu = \mathrm{O}(1)$ reduces the range of curvatures to be considered at high Reynolds numbers.

C. Euler equations

The Euler equations which are supposed to be a good approximation in the core flow, far from the boundary layers, are formally obtained for a high Reynolds number and a small median line curvature.

Since non-linear terms are small in the core flow, and since we seek for $\mathrm{O}(\delta)$ approximations, we thus use the linearized Euler equations. We then have,

$$\frac{\partial u_1}{\partial X} + \frac{\partial v_1}{\partial Y} = 0, \tag{29}$$

$$u_0\frac{\partial u_1}{\partial X} + v_1\frac{du_0}{dY} = -\frac{\partial p_1}{\partial X}, \tag{30}$$

$$u_0\frac{\partial v_1}{\partial X} - ku_0^2 = -\frac{\partial p_1}{\partial Y}. \tag{31}$$

We know from preceding analysis (Cousteix and Mauss[14]) that u_1 has a logarithmic singularity near the boundaries. Thus, a classical asymptotic method using matching will not work easily.

Since in Eqs. (29) and (30), only the derivative in X of u_1 appears, we use the equation,

$$-u_0\frac{\partial v_1}{\partial Y}+v_1\frac{du_0}{dY}=-\frac{\partial p_1}{\partial X} \tag{32}$$

instead of the Eqs. (29) and (30).

D. The pressure

We now show that the additional contribution P_{BL} to the pressure in the boundary layer is negligible in comparison to the pressure p_1 which satisfies the linearized Euler model (Eqs. (31) and (32)) of the core flow.

To satisfy the boundary condition $V=0$, it is required, from Eq. (23), that $v_1=\mathrm{O}(\varepsilon)$ in the boundary layer. Thus, by analysing the behaviour of the core pressure *in the boundary layer*, through (Eqs. (31) and (32)), we obtain that

$$\frac{\partial p_1}{\partial X}=\mathrm{O}(\varepsilon)\quad\text{and}\quad\frac{\partial p_1}{\partial Y}=\mathrm{O}(\varepsilon^2). \tag{33}$$

Since the transverse momentum Eq. (18) shows that $\frac{\partial P}{\partial Y}=\mathrm{O}(\varepsilon^3)$ in the boundary layer, Eq. (24) implies that $\Delta=\mathrm{O}(\varepsilon^3)$. It can also be seen, from the same Eq. (24), that in the whole field (boundary layer and core),

$$\frac{\partial P}{\partial X}=\frac{\mathrm{d}p_0}{\mathrm{d}X}+\delta\left(\frac{\partial p_1}{\partial X}+\mathrm{O}(\varepsilon^3)\right). \tag{34}$$

This result is the key of the analysis since, at the considered order, in Eq. (17), $\frac{\partial P}{\partial X}$ can be replaced by $\frac{\partial P_1}{\partial X}$, where

$$\frac{\partial P_1}{\partial X}=\frac{\mathrm{d}p_0}{\mathrm{d}X}+\delta\frac{\partial p_1}{\partial X}. \tag{35}$$

As far as the driving pressure gradient is concerned, the inertial effects of the perturbation in the core region are shown to be many orders more important than those induced directly by the perturbation in the boundary layer region. These modifications are not simply transmitted to the boundary layer but negotiated through a strong coupling.

V. THE GIBL

A. General formulation

To build the model, we may be tempted by more traditional methods suggested by the expressions (22) and (23), namely write the equations for U_{BL} and V_{BL} and use the principles of regular asymptotic developments to match zones between the core and boundary layer. Knowing that (u_1,v_1) is an approximation of the solution in the core flow, we can use the matching conditions,

$$\lim_{\eta\to\infty}U_{BL}=0\quad\text{and}\quad\lim_{\eta\to\infty}V_{BL}=0 \tag{36}$$

to solve the equations. In fact, by using the SCEM as described in Sec. IV B, the equations reduce in the boundary layer to,

$$\frac{\partial U}{\partial X}+\frac{\partial V}{\partial Y}=0, \tag{37}$$

$$U\frac{\partial U}{\partial X}+V\frac{\partial U}{\partial Y}=-\frac{\partial P_1}{\partial X}+\frac{1}{R_e}\frac{\partial}{\partial Y}\left[(1+KY)\frac{\partial U}{\partial Y}\right]. \tag{38}$$

The $\frac{1+KY}{R_e}$ term in Eq. (38) can be interpreted as an algebraic variable viscosity induced by the curvature.

The same Eqs. (37) and (38) and the same results for the pressure can be obtained for the upper wall. Therefore, it is clear that (Eqs. (37) and (38)) associated with the core flow, Eqs. (31) and (32) give an approximation valid in the whole channel, a UVA.

These equations are associated with the boundary conditions (6).

As the full model comprises the generalized boundary layer Eqs. (37) and (38) for U, V and the core flow Eqs. (31) and (32) for v_1 and p_1 with boundary conditions (6), we must link the two sets of equations. This is achieved by the fact that the uniformly valid approximation V must agree with $V_1 = \delta v_1$ in the core. This is not a matching condition, but somewhere in the core, for $Y = Y_c$, we impose,

$$V = V_1. \tag{39}$$

This can be done for instance on the median line with $Y_c = 0$.

This GIBL problem is easier to formulate than a more classical matched asymptotic method. This is a reason why we use U and V, in Eqs. (22) and (23) instead of the boundary layer variables U_{BL} and V_{BL}.

The field Eqs. (37) and (38) have the same form as Prandtl equations, however, these equations are no more boundary layer equations, and they are *uniformly valid in the whole field of the flow*.

B. A simplified model

When the influence length, L^*, of the perturbation in the flow field is larger than the channel height H, the pressure X-derivative can be neglected in Eq. (30) (see Appendix B). Then, the solution of Eqs. (29) and (30) is

$$u_1 = A(X)u_0', \quad v_1 = -u_0 A'(X), \tag{40}$$

where A is yet an unknown function.

The fact that v_1 is symmetric corresponds to an antisymmetric geometrical configuration which is the case treated here.

By replacing the expressions (40) into Eq. (31), we obtain that

$$-u_0^2 A''(X) - k u_0^2 = -\frac{\partial p_1}{\partial Y}, \tag{41}$$

which permits to calculate the pressure,

$$p_1 = (A'' + k)\int_{Y_c}^{Y} u_0^2(Y')\,\mathrm{d}Y' + B(X). \tag{42}$$

Thus, from Eq. (35), we can write

$$\frac{\partial P_1}{\partial X} = \frac{\mathrm{d}p_0}{\mathrm{d}X} + \delta(A''' + k')\int_{Y_c}^{Y} u_0^2(Y')\,\mathrm{d}Y' + \delta B'(X). \tag{43}$$

In order to treat curvature discontinuities, we use a change of variables such as neither k or k' appears in the equations (see Appendix C).

C. Numerical procedure

According to the analysis proposed in Sec. V A, the problem is to solve the generalized boundary layer Eqs. (37) and (38) associated to the core flow Eqs. (31) and (32). The velocity components U and V vanish at the walls and the coupling condition between the boundary layer

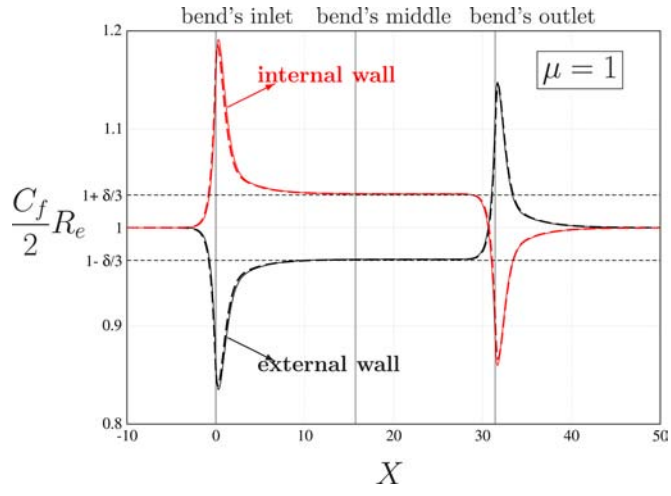

FIG. 2. (Color online) Nondimensional wall shear stress, $\frac{C_f}{2}R_e$, with respect to the distance along the median curve, X; the long dashed lines give the approximate levels of the established flow wall shear stress in the bend, $1 \pm \delta/3$; $R_c = 10H$ and $R_e = 1000$; and straight lines: NS results and dashed lines: GIBL results.

solution and the core flow solution is given by Eq. (39). More details about the numerical resolution of these GIBL equations can be found in Cathalifaud *et al.*[15]

By using the model described in Sec. V B, we obtain a simplified GIBL problem which is made of Eqs. (37), (38), and (43). In this formulation, we have to determine $A(X)$ and $B(X)$. To this end, two conditions are used: the first one is to ensure mass flow conservation in the channel and the second one is given by the coupling condition (39).

A step by step marching procedure from upstream to downstream is used to calculate U and V. Several sweeps of the calculation domain are required in order to take into account the upstream influence. At a given station X_s, as a first approximation, it is assumed that the function A is known. The solution of the generalized boundary layer equations is determined by iterating on the value of function B at the considered station in order to ensure global mass flow conservation in the channel, i.e., to satisfy $V = 0$ on both walls. More precisely, the derivative $\frac{dB}{dX}$, which is present in the momentum equation, is determined. Upon convergence, an updated value of A is calculated as follows. The continuity equation is integrated between the lower wall $Y = -1/2$ and the median line $Y_c = 0$ by taking into account the core condition (39), the boundary condition $V(-1/2) = 0$, and the relation (40), which gives the updated value of A as

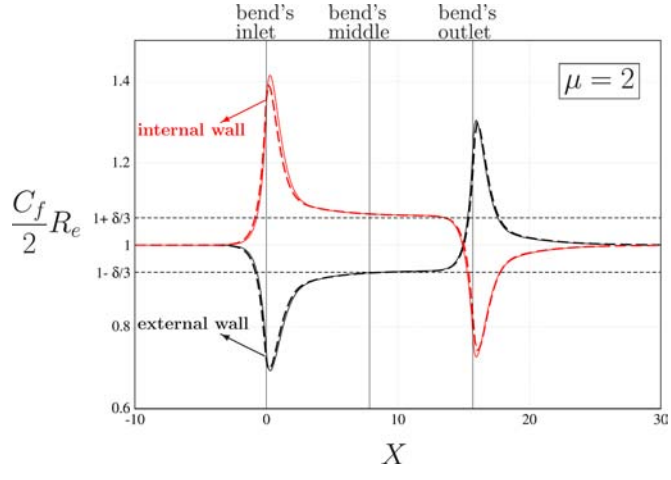

FIG. 3. (Color online) Nondimensional wall shear stress, $\frac{C_f}{2}R_e$, with respect to the distance along the median curve, X; the long dashed lines give the approximate levels of the established flow wall shear stress in the bend, $1 \pm \delta/3$; $R_c = 5H$ and $R_e = 1000$; and straight lines: NS results and dashed lines: GIBL results.

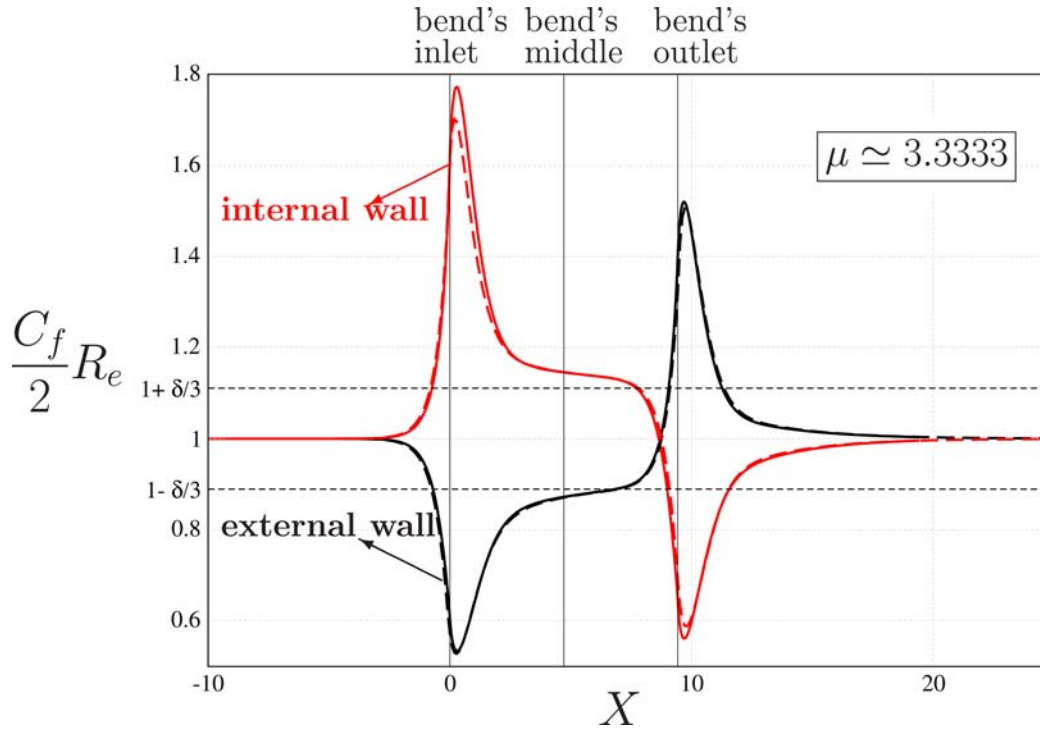

FIG. 4. (Color online) Nondimensional wall shear stress, $\frac{C_f}{2}R_e$, with respect to the distance along the median curve, X; the long dashed lines give the approximate levels of the established flow wall shear stress in the bend, $1 \pm \delta/3$; $R_c = 3H$ and $R_e = 1000$; and straight lines: NS results and dashed lines: GIBL results.

$$\frac{\mathrm{d}A}{\mathrm{d}X} = \frac{1}{u_0(Y_c)} \int_{-1/2}^{Y_c} \frac{\partial U}{\partial X} d\eta. \tag{44}$$

When the updated value of A is determined, the calculations proceed to the next station. The updated value of A is used at the next sweep. More details about the resolution of this simplified GIBL model can be found in Cousteix and Mauss.[16]

VI. RESULTS

To test the validity of the GIBL model for curved channels, we consider a geometrical configuration that includes tangent straight channels upstream and downstream of a 180° curved part. The straight parts have been added to avoid the problem of inlet and outlet boundary conditions at the entry and exit of the curved part which are not known *a priori*. Even the fully established curved solution as inlet condition to the curved channel would seem non physical since it would mean that the curved channel is virtually longer upstream than it is actually and that the flow has been fully established. In fact any inlet boundary condition at the entry of the curved part alone creates a cut off of the upstream non linear interaction. This configuration allows also to test the effect of a curvature discontinuity.

At the inlet of the upstream straight channel, a parabolic profile was given while at the outlet of the downstream straight channel a constant zero pressure was prescribed. This configuration has also been chosen to explore the upstream influence as well as the downstream effects before and after the curved part. Several curvatures ranging from 0.1 to 1 as well as different values of the Reynolds number R_e ranging from 1 to 10 000 have been investigated. The NS equations have been solved using commercial softwares FLUENT or COMSOL which gave similar results for the cases treated here. The lengths of the straight parts of the channels were varied from $10H$ to $20H$ for the upstream part and from $10H$ to $70\pi H$ for the downstream part depending on the Reynolds number to recover an established Poiseuille flow at the outlet.

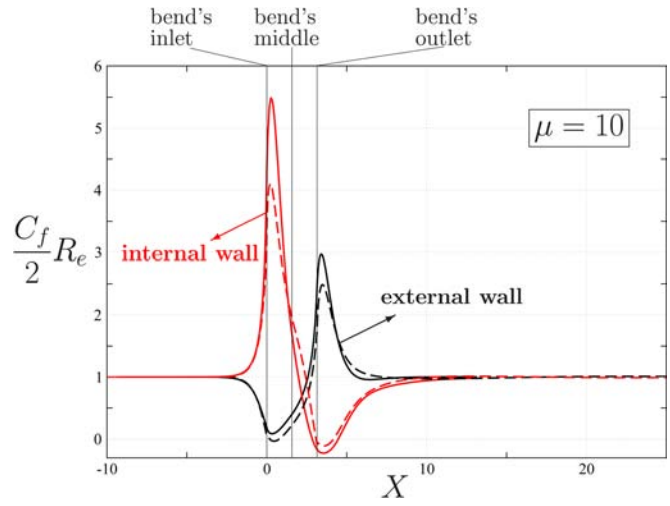

FIG. 5. (Color online) Nondimensional wall shear stress, $\frac{C_f}{2}R_e$, with respect to the distance along the median curve, X; $R_c = H$ and $R_e = 1000$; and straight lines: NS results and dashed lines: GIBL results.

A. Shear stress

The skin friction coefficient which is the non dimensional wall shear stress τ_w,

$$C_f = \frac{\tau_w}{\frac{1}{2}\rho U^{*2}} \tag{45}$$

is known as a very sensitive characteristic of the flow field. For our case, we have,

$$C_f = \mp \frac{2}{R_e}\frac{\partial U}{\partial Y}\bigg|_{Y=\pm\frac{1}{2}}. \tag{46}$$

Figures 2 to 10 present several cases where the shear stress obtained by the GIBL model is compared to the numerical solution of the complete NS equations. As can be seen qualitative global behaviour as well as quantitative predictions of the shear stress at both walls is well reproduced by the GIBL model for small curvatures δ up to 0.3 and $R_e = 1000$ when compared to complete NS. The accuracy of the GIBL model depends on the key parameter $\mu = \delta R_e^{\frac{1}{3}}$ since this asymptotic model was build under the assumption that μ is O(1). But even when $\mu = 10$, i.e., when

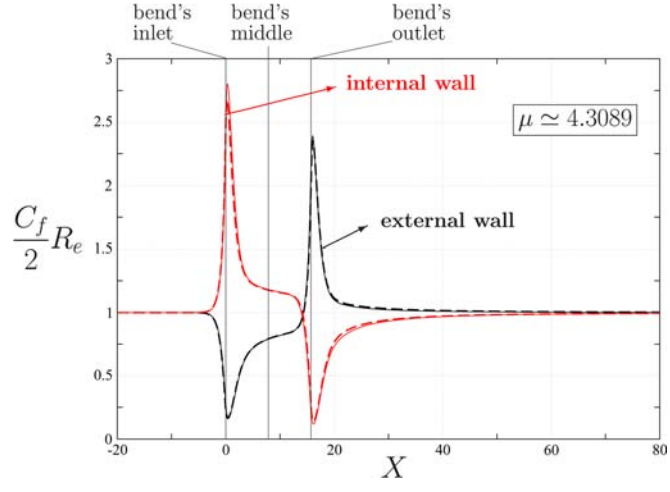

FIG. 6. (Color online) Nondimensional wall shear stress, $\frac{C_f}{2}R_e$, with respect to the distance along the median curve, X; $R_c = 5H$ and $R_e = 10\,000$; and straight lines: NS results and dashed lines: GIBL results.

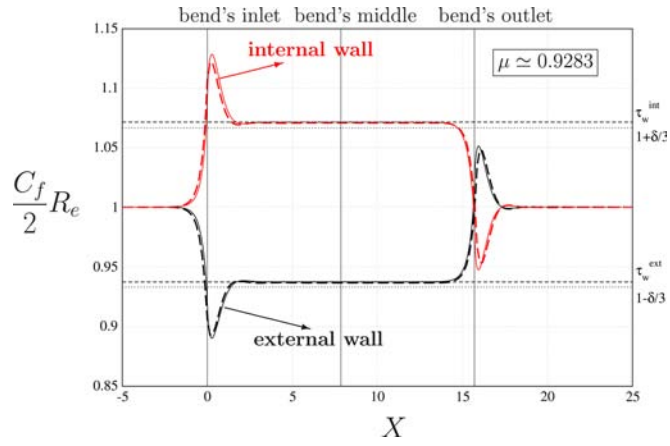

FIG. 7. (Color online) Nondimensional wall shear stress, $\frac{C_f}{2}R_e$, with respect to the distance along the median curve, X; the long dotted and dashed lines give, respectively, the approximate $(1 \pm \delta/3)$ and the exact (τ_w^{int} and τ_w^{ext}) levels of the established flow wall shear stress in the bend; $R_c = 5H$ and $R_e = 100$; and straight lines: NS results and dashed lines: GIBL results.

$\delta = 1$ (Figure 5), which is out of the formal range of validity of the GIBL model, since it was formally constructed on the basis of a small curvature, one can see that the upstream effect is accurately captured. As for the peaks that appear at the vicinity of the entry of the curved part, the small difference in the cases where $\delta \leq 0.3$ might be due to the simplified expression (43) used in the GIBL instead of solving the pressure Poisson equation or to the discontinuity of the curvature at the junctions of the straight parts with the curved one.

The normalised shear stress $\frac{C_f}{2}R_e$ increases at the internal wall and decreases at the external wall relatively to the upstream Poiseuille flow and then tends asymptotically to the established solution (where $C_f = \mp \frac{2}{R_e}\frac{dU_0}{dY}\big|_{Y=\pm\frac{1}{2}}$) for $\delta \leq 0.3$ whenever a fully established flow zone does potentially exist which is R_e and δ dependent. The approximate established values for the wall shear stress $1 \mp \frac{\delta}{3}$, deduced from the simplified Eq. (11), are plotted as straight dashed lines in some figures.

It should be mentioned that the fully established values for NS and GIBL C_f are numerically slightly different since the basic equations for the established flows differ as *the solved NS equations neglect no terms involving* δ while GIBL model neglects formally the δ^2 term in the basic

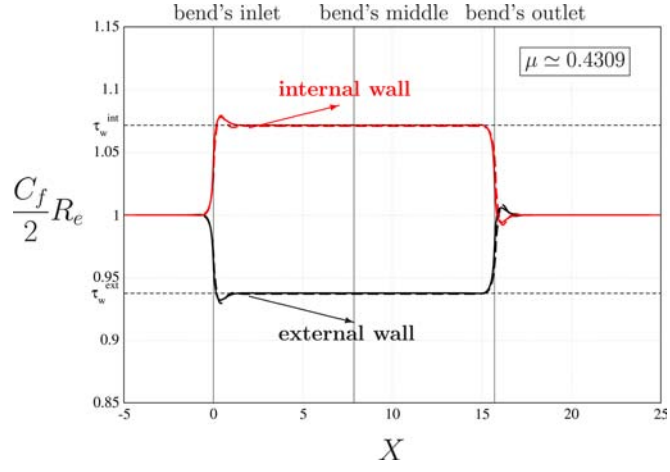

FIG. 8. (Color online) Nondimensional wall shear stress, $\frac{C_f}{2}R_e$, with respect to the distance along the median curve, X; the long dashed lines give the exact levels of the established flow wall shear stress in the bend, τ_w^{int} and τ_w^{ext}; $R_c = 5H$ and $R_e = 10$; and straight lines: NS results and dashed lines: GIBL results.

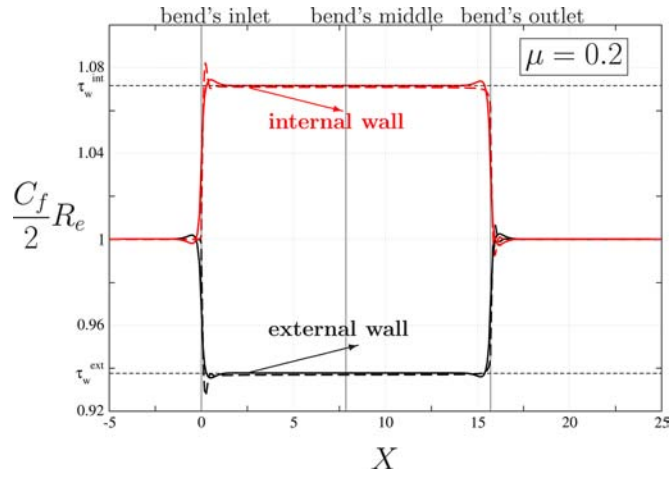

FIG. 9. (Color online) Nondimensional wall shear stress, $\frac{C_f}{2}R_e$, with respect to the distance along the median curve, X; the long dashed lines give the exact levels of the established flow wall shear stress in the bend, τ_w^{int} and τ_w^{ext}; $R_c = 5H$ and $R_e = 1$; and straight lines: NS results and dashed lines: GIBL results.

equation but happens to keep in its solution some terms involving δ^2 through logarithmic terms. It has been shown above that the NS equations, whatever are the values of R_e or δ reduce in the fully established zone to the Eq. (7), whose analytical solution is Eq. (8). It is expected that the solution of the complete NS equations will tend asymptotically to these values in the established zone. This is somewhat the case as can be seen in the figures.

The GIBL formally tends in the fully established zone to Eq. (9), whose analytical solution is Eq. (10). The differences between the fully established GIBL and NS wall shear stress are of the order 10^{-3}.

After these plateau regions, when they exist, an opposite behaviour follows before the exit of the curved channel rendering the second upstream influence of the transition from curved to straight channel. Downstream in the straight channel the Poiseuille case is recovered at some distances from the outlet, being longer as Re is higher. We found it necessary to expand the downstream channel up to $70\pi H$ to reach an established Poiseuille flow at about $40H$ for $R_e = 10\,000$ and $\delta = 0.2$ (see Figure 6).

Other values than $R_e = 1000$ or $R_e = 10\,000$ were tested. Since The GIBL was formally established for high Reynolds number, and mainly in the core region where linear Euler equations were used, it was tempting to test whether this GIBL can provide accurate results for smaller R_e. In

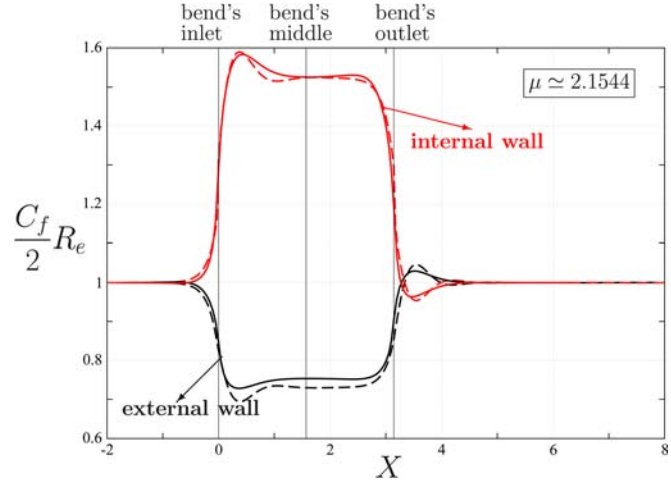

FIG. 10. (Color online) Nondimensional wall shear stress, $\frac{C_f}{2}R_e$, with respect to the distance along the median curve, X; $R_c = H$ and $R_e = 10$; straight lines: NS results and dashed lines: GIBL results.

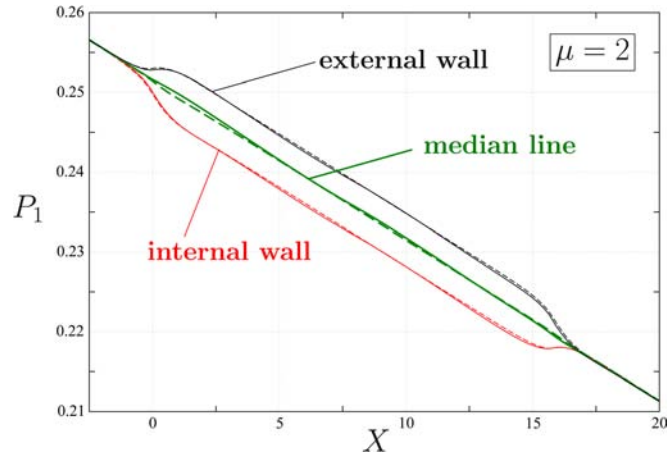

FIG. 11. (Color online) Pressure P_1 with respect to the distance along the median curve, X; $R_c = 5H$ and $R_e = 1000$; and straight lines: NS results and dashed lines: GIBL results.

Figures 7 to 9, it can be seen that this is the case for $R_e = 100$, $R_e = 10$, and $R_e = 1$ for $\delta = 0.2$ and even for $\delta = 1$ when $R_e = 10$ in Figure 10 which is apparently a surprising result. However, although R_e and δ are the fundamental parameters for this asymptotic model, it is their combination in $\mu = \delta R_e^{\frac{1}{3}}$ which acts as a global model "lock" that ultimately determine the accuracy of this GIBL model. Very often asymptotically and rationally built models achieve such accuracy out of the domain of their expected hypothetical validity.

B. Pressure distribution

The pressure evolution at the walls and in the median line through the tangent and curved parts is well reproduced by the GIBL as can be seen in Figure 11 for $R_e = 1000$ and $\delta = 0.2$. The less apparent agreement in the curved part as R_e is increased to 10 000 is due mainly to scaling factors since Figure 11 deals with values ten times greater than Figure 12. Its general behaviour is similar to the curve obtained experimentally by Ito[17] in the $3D$ pipe case and for higher R_e. Our $2D$ simulation shows clearly how the curvature of the bend is involved in the whole structure of the fluid motion characteristics *in the absence of the azimuthal secondary flow phenomenon* and may be used to distinguish the pure $3D$ aspects from the $2D$ ones. In fact in the literature one is uncomfortable by what the authors put under the expression *"secondary flow"* since this is sometimes mainly related to *the azimuthal* secondary flow initiated in the transverse boundary layer by the "centrifugal" forces. However, as the $2D$ clearly shows the "centrifugal" forces give rise to an

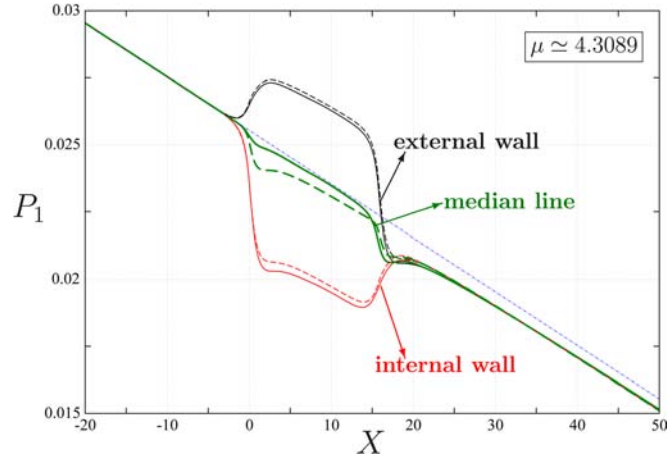

FIG. 12. (Color online) Pressure P_1 with respect to the distance along the median curve, X; $R_c = 5H$ and $R_e = 10\ 000$; straight lines: NS results; dashed lines: GIBL results; and dot-dashed line: equivalent straight channel pressure.

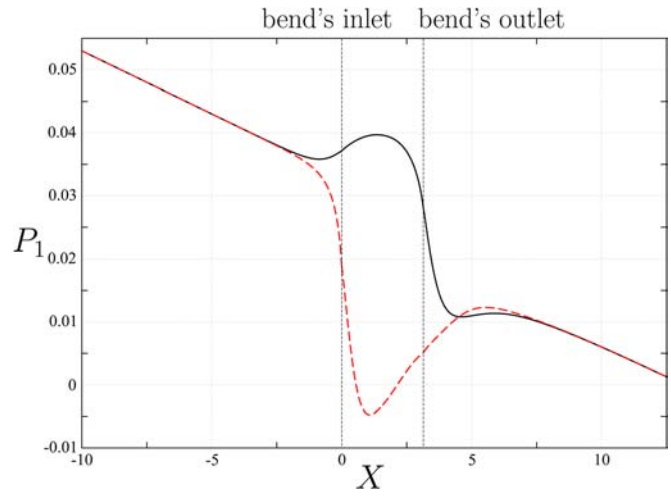

FIG. 13. (Color online) Pressure P_1 with respect to the distance along the median curve, X; $R_c = 1H$ and $R_e = 1000$ (NS results); and straight lines: external wall and dashed lines: internal wall.

in plane displacement initiated by the curvature and this suffices to reproduce qualitatively the main salient characteristics that Ito's pressure curves (measured experimentally) exhibit. Both this displacement and the azimuthal secondary flow are manifestations of the curvature in the $3D$ case but the former is sometimes put aside or not enough highlighted.

Variations in pressure due to the presence of the bend start to occur in the upstream tangent channel at some distance away from the bend, and we note that this upstream effect induced by the presence of the distal curved part is captured clearly and accurately by the GIBL model. In the upper boundary layer near the internal wall, the pressure drops and in the lower boundary layer near the external wall the pressure rises in the straight tangent part in anticipation before the curved part is reached. The physical scenario of this upstream influence induced here by the bend is well and deeply analysed by Smith,[18] whatever the accident is, in this way: *In physical terms, the small increase in pressure near the lower wall causes the viscous layer there to expand, and consequently the upper layer to contract, a motion which sets up a negative pressure gradient across the channel. This produces a small decrease in pressure near the upper wall, tending to induce an even greater compression of the viscous layer there, and so the process is reinforced.*

In the continuation of the upstream effect, an adverse pressure gradient develops on the outer wall of the bend and a favourable gradient is formed on the inner wall. At about the bend's exit,

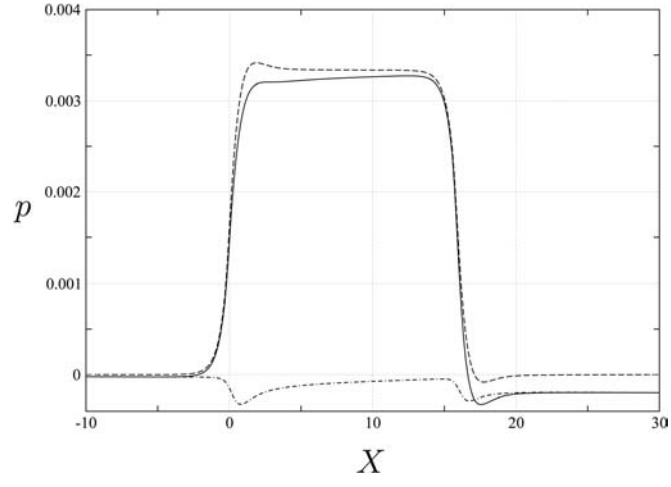

FIG. 14. Pressure p at the external wall with respect to the distance along the median curve, X; $R_c = 5H$ and $R_e = 1000$ (GIBL); and straight line: p, dashed line: $(A'' + \delta) \int_{Y_c}^{\text{wall}} u_0^2 \, dy$, and dot-dashed line: $B - P_0$.

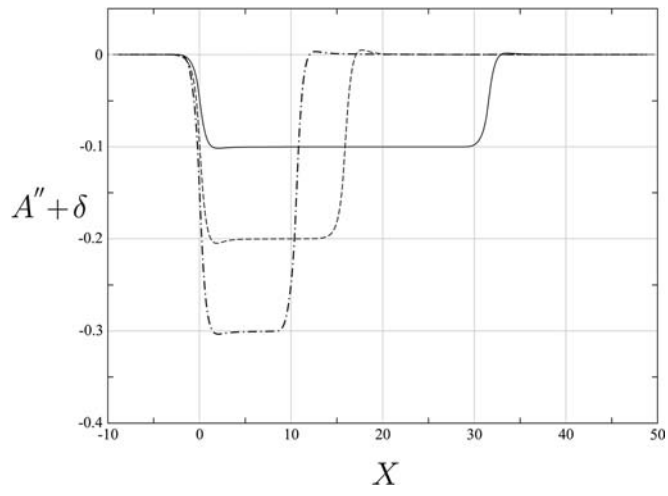

FIG. 15. $A'' + \delta$ with respect to the distance along the median curve, X, for different values of δ; $R_e = 1000$ (GIBL); straight line: $\delta = 0.1$; dashed line: $\delta = 0.2$; and dot-dashed line: $\delta = 0.3$.

the situation is inverted: it is at the inner wall that the adverse pressure gradient is set. It is in these zones of adverse pressure gradients that separation may occur as can be seen in Figure 5 where separation is located around the exit at the internal wall. The adverse pressure gradient at the outer wall near the bend's entry being less than the adverse gradient at the inner wall near the bend's exit (see Figure 13) may explain that separation is initiated at the exit and not at the entry in this case.

It is interesting to analyse the pressure evolution using the approximation of Eq. (42) which involve the 3 parameters $A''(X)$, δ, and $B(X)$. The main contribution comes from the $(A'' + \delta) \int_{Y_c}^{\text{wall}} u_0^2 \, dy$ term as shown in Figure 14. Whenever the fully developed flow is established in the straight parts, this term vanishes due to the vanishing of both δ and $A''(X)$. If the fully developed flow is established in the curved part, only $A''(X)$ is zero, due to the vanishing of $\frac{\partial v_1}{\partial X}$ and the transverse pressure gradient is solely balanced by the so called centrifugal forces, i.e., δu_0^2. We thus recover in the curved established flow δ as the only non zero coefficient of the integral term involved in the pressure. This can be seen clearly in Figure 15.

The sharp variations due to the discontinuity of the curvature at both junctions between the curved part and the straight tangent channels are well captured by the GIBL as can be illustrated through the displacement function $A(X)$ which is related to the core longitudinal velocity perturbation, and hence also by $A'(X)$ which is related to the transverse velocity and by $A''(X)$ as can be seen in Figure 16. All of them are zero when the flow is established in the straight parts, but only $A'(X)$ and $A''(X)$ are null in the curved part. $A(X)$ does not vanish in the curved part since the fully established curved flow is considered by GIBL as a perturbation relative to the local Poiseuille flow.

In the downstream tangent straight channel, a linear pressure decrease, with the displacement effect A tending to zero, is recovered in a more or less longer length depending on the R_e value. A Poiseuille flow like situation was almost attained at a $40H$ length in the downstream straight tangent channel for the case of $R_e = 10\,000$.

C. Velocity profiles and upstream influence length

The evolution of the radial velocity and the axial perturbation velocity profiles in the upstream tangent channel proximal to the bend's entry are presented in Figure 17. The influence of the bend on the velocities distribution is shown to exist a few diameters upstream of the bend. The extension of this upstream influence is well captured by the GIBL model. The amplitude of the velocity perturbations seems more accurately reproduced by the GIBL for the radial velocity than for the axial perturbation. The fluid near the inner wall accelerates relatively to Poiseuille flow in the inner wall and decelerates at the outer wall while the maximum of the radial velocity is

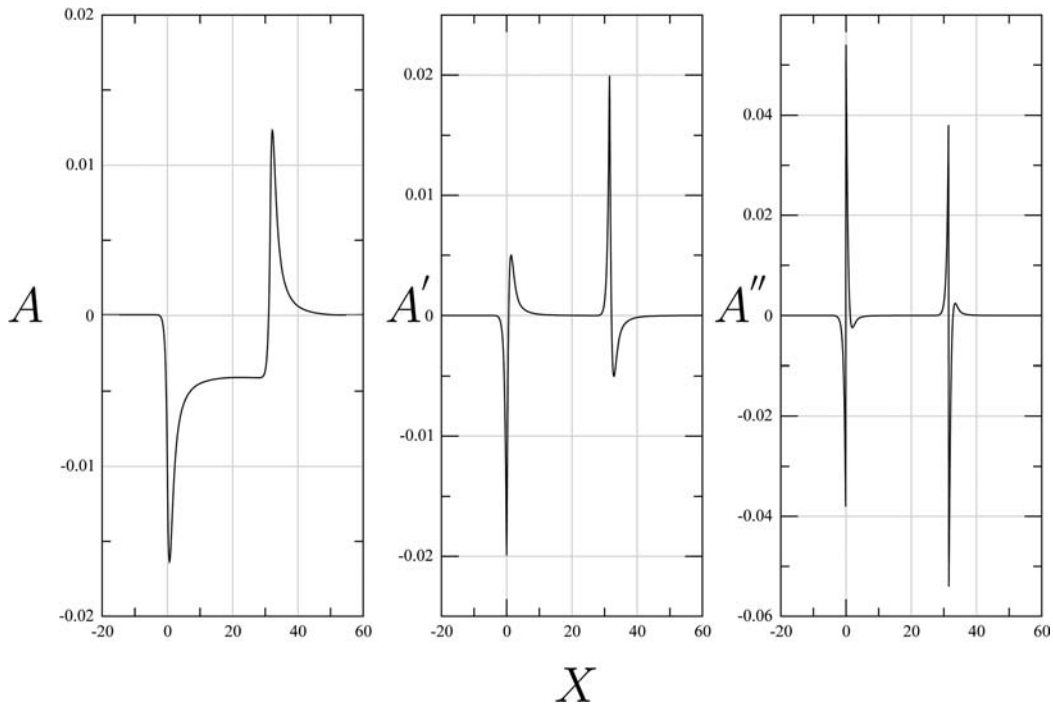

FIG. 16. A, A', and A'' with respect to the distance along the median curve, X, for the case $R_c = 10H$ and $R_e = 1000$ (GIBL).

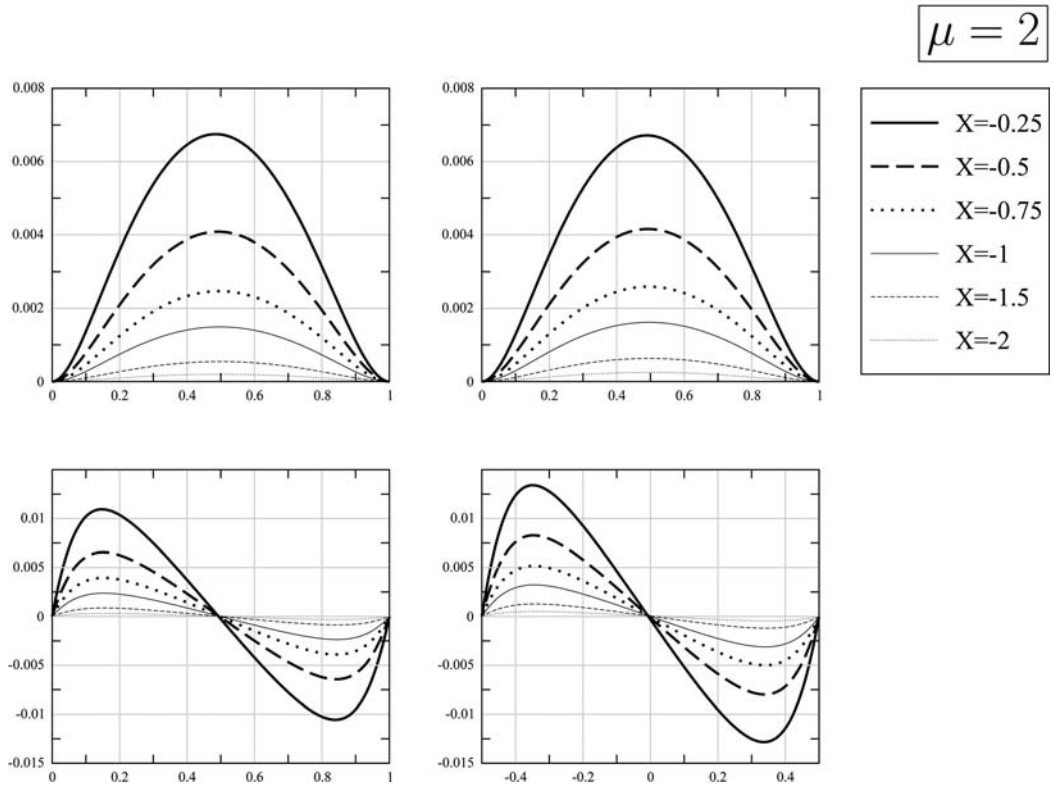

FIG. 17. $v(X,\eta)$ (top) and $u(X,\eta)$ (bottom) profiles upstream the bend, for different values of X (from -2 to -0.25); $R_c = 5H$ and $R_e = 1000$; and left (NS) and right (GIBL).

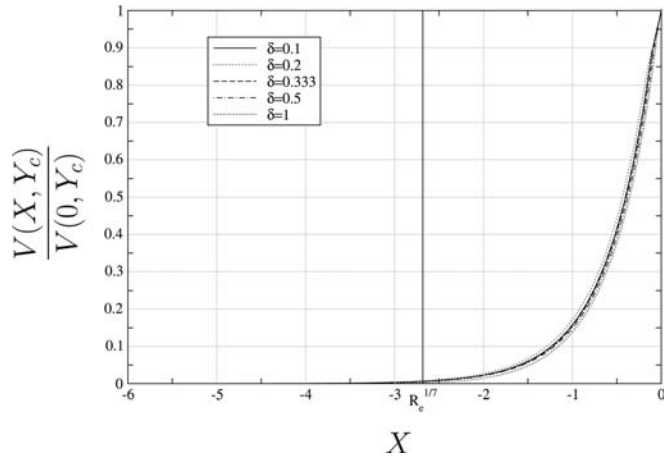

FIG. 18. Normalized $V(X,Y_c)$ with respect to the distance along the median curve, X, for different values of δ (from 0.1 to 1); $R_e = 1000$ (GIBL).

at the center of the channel. Thus, a skewing of the velocity profile towards the inner wall is induced in anticipation and before the curved part is reached. This shows that imposing a flat profile at the entry of a curved channel as was done previously by Snyder and Lovely[9] may appear somewhat artificial since it does not take into account the upstream effect. Adopting the geometrical configuration of a bend having a proximal tangent channel circumvents the problem of the bend inlet condition even though this configuration does introduce a discontinuous curvature at the junction of the straight channel to the bend. The bends inlet flow condition is, therefore, solved while taking into account the free upstream non linear interaction.

The length of this upstream influence to an incoming Poiseuille flow was shown asymptotically to be, for high Reynolds, of the order of $R_e^{\frac{1}{7}}$ by Smith[18] whatever the nature of the distal perturbation is. In the present work, it was found numerically by solving NS or GIBL that this upstream length is of the order of $R_e^{\frac{1}{7}}$ for the $R_e = 1000$ whatever the curvature is as can be seen in Figure 18. Moreover, this is the case also for R_e ranging from 100 to 10 000 (Figures 19 and 20). However, this is not the case for $R_e \preceq 10$ (Figure 19). This confirms and validates the high Reynolds asymptotic analysis performed by Smith for the upstream effects and mainly its length. This may have important implications in situations involving the flow control.

Figures 21 and 22 present the cross section evolutions of the axial, transverse velocities, and pressures at 3 stations in the curved pipe. The higher axial velocities at a cross section occur on the inner wall at the bend entry and on the outer wall at the bend exit. Near the walls, the

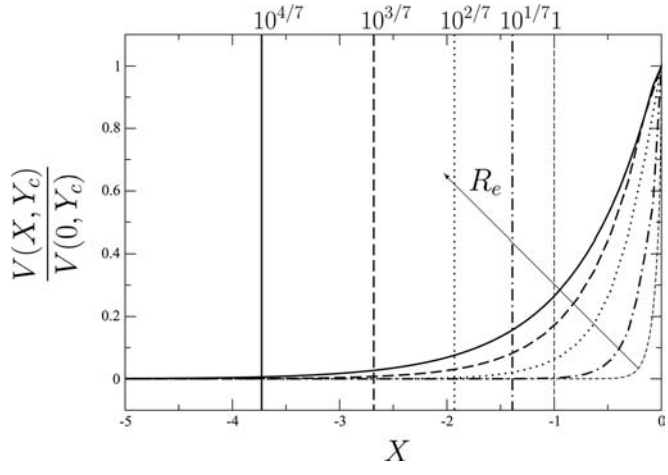

FIG. 19. Normalized $V(X,Y_c)$ with respect to the distance along the median curve, X, for different values of R_e (from 1 to 10 000); $\delta = 0.2$ (GIBL).

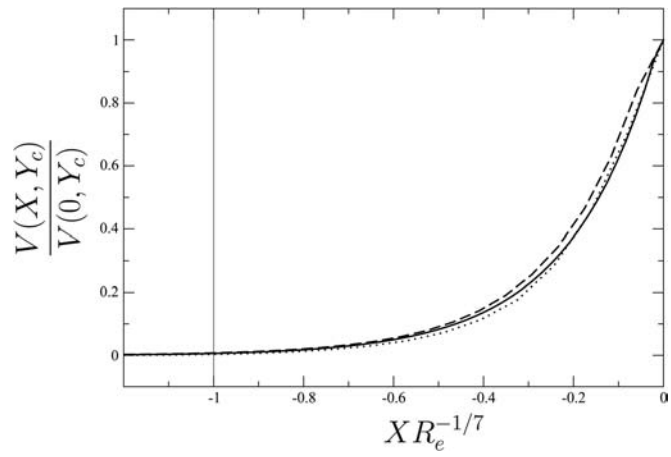

FIG. 20. Normalized $V(X,Y_c)$ with respect to the normalized distance along the median curve, $XR_e^{-\frac{1}{7}}$, for different values of R_e (from 100 to 10 000); $\delta = 0.2$ (GIBL).

agreement between the GIBL and NS plots is very good compared to the core flow at the extremities of the bend where more differences are apparent. This seems mainly due to the discontinuity of the curvature at the bend extremities rather than to the linear Euler approach used in the core region to compute the pressure since in the middle of the bend the GIBL and the NS results match better.

VII. CONCLUSION

Through an asymptotic process, a uniformly valid asymptotic model for curved 2D channel flows was obtained. This reduced model, termed GIBL for global interactive boundary layer, was used to investigate the flow characteristics in a configuration including a 180° channel bend of constant curvature connected to two tangent upstream and downstream straight channels. This configuration makes it possible to overcome the difficult problem of what inlet or outlet conditions

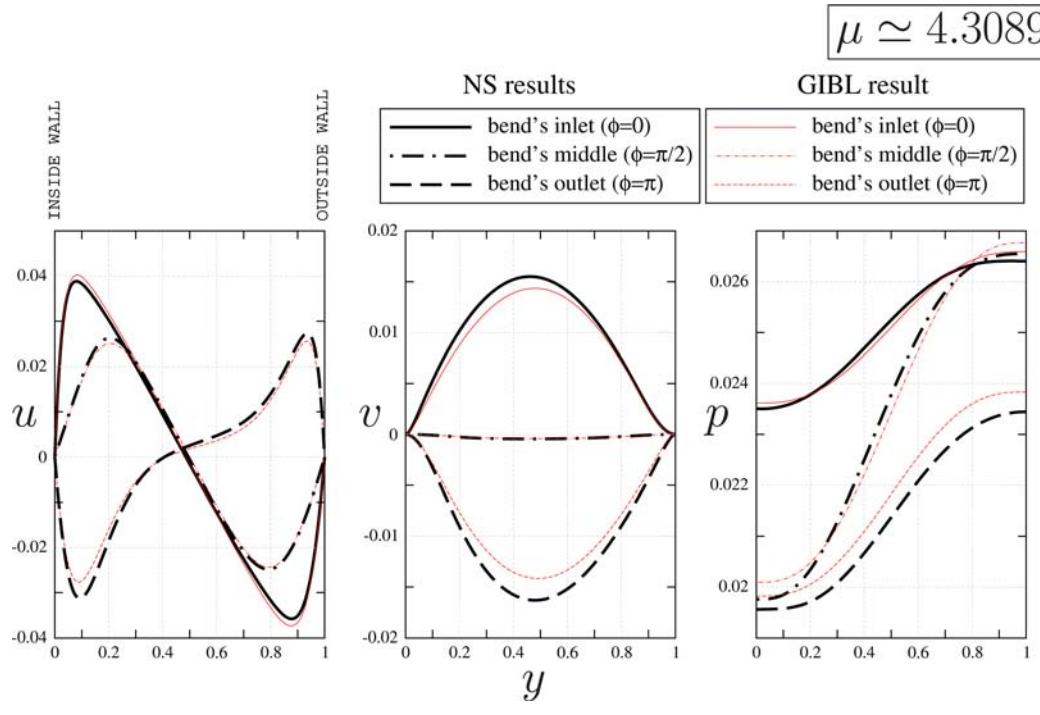

FIG. 21. (Color online) u, v, and p profiles; $R_c = 5H$ and $R_e = 10\,000$.

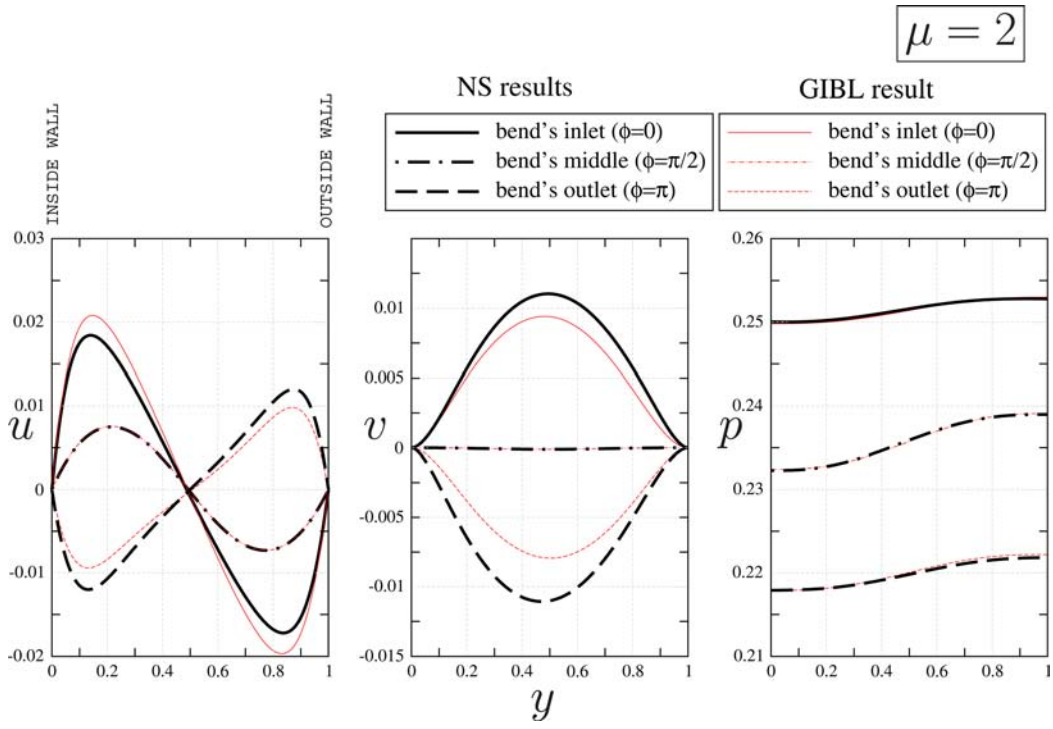

FIG. 22. (Color online) u, v, and p profiles; $R_c = 5H$ and $R_e = 1000$.

are to be imposed numerically at the bend's extremities, thus leaving the non linear upstream and downstream interactions develop freely. Unlike the triple deck boundary layer's equations where the transverse Y variable is local, i.e., a boundary layer variable, the GIBL model deals with a global Y that varies through the entire channel section. The other important feature of the model presented in this paper is that it also deals with a global X that varies through the entire channel longitudinal length (from entry to outlet). This GIBL model was constructed for a high Reynolds number laminar channel flow with the bend being considered as a perturbing situation to an otherwise fully developed Poiseuille flow. Another perturbation is due to the discontinuous curvature at the bend's extremities.

The bend's curvature is assumed small but the controlling parameter of this asymptotic model is the non-dimensional number $\mu = \delta R_e^{\frac{1}{3}}$ which is supposed O(1). As long as this condition is satisfied, the GIBL is in good agreement with the full Navier-Stokes simulations even for small R_e cases. Satisfactory predictions for the wall shear stress, pressure distribution, axial and radial velocities through the whole configuration were obtained. This was achieved even when using a simplified Euler model, proposed by Stewartson and Williams[19] for the external flow and rationally formulated for the internal flow by Smith, instead of solving the Poisson equation for the pressure.

A future task would be to explore the flow characteristics of variable curvature and/or variable section height before extending this approach to the most challenging case, i.e., the 3D pipe case where secondary flow occurs and induces more complex interaction.

APPENDIX A: NAVIER-STOKES EQUATIONS IN GENERALIZED COORDINATES

For a point M with general coordinates X and Y, we can write $\overrightarrow{OM} = \overrightarrow{OM_0} + Y\vec{n}$, where $\vec{n}$ is the unit normal vector. Then,

$$\overrightarrow{\mathrm{d}M} = \mathrm{d}X(1 + KY)\vec{\tau} + \mathrm{d}Y\vec{n},$$

where $\vec{\tau}$ is the unit vector tangent at M_0 to the median line in such a way that the orientation of $(\vec{\tau}, \vec{n})$ is positive or right-handed; $K(X)$ is the algebraic curvature of this line.

Thus, the continuity equation and the Cauchy equations may be written as

$$\frac{\partial U}{\partial X}+\frac{\partial}{\partial Y}[(1+KY)V]=0, \tag{A1}$$

$$U\frac{\partial U}{\partial X}+(1+KY)V\frac{\partial U}{\partial Y}+KUV=-\frac{\partial P}{\partial X}+\left[\frac{\partial \sigma_{XX}}{\partial X}+\frac{\partial}{\partial Y}(1+KY)\sigma_{XY}+K\sigma_{XY}\right], \tag{A2}$$

$$\frac{1}{1+KY}U\frac{\partial V}{\partial X}+V\frac{\partial V}{\partial Y}-\frac{K}{1+KY}U^2=-\frac{\partial P}{\partial Y} +\frac{1}{1+KY}\left[\frac{\partial \sigma_{XY}}{\partial X}+\frac{\partial}{\partial Y}(1+KY)\sigma_{YY}-K\sigma_{XX}\right], \tag{A3}$$

where, for a newtonian fluid, we have

$$\sigma_{XX}=\frac{2}{(1+KY)R_e}\left(\frac{\partial U}{\partial X}+KV\right), \tag{A4}$$

$$\sigma_{XY}=\frac{1}{(1+KY)R_e}\left(\frac{\partial V}{\partial X}+(1+KY)\frac{\partial U}{\partial Y}-KU\right), \tag{A5}$$

$$\sigma_{YY}=\frac{2}{R_e}\frac{\partial V}{\partial Y}. \tag{A6}$$

We assume that K is a small parameter. Since we are considering a high Reynolds number basic flow dominated by its longitudinal component, all the terms are small except U, $\frac{\partial U}{\partial Y}$, $\frac{\partial^2 U}{\partial Y^2}$, and $\frac{\partial P}{\partial X}$ which are of order 1.

Let say that K, V, $\frac{\partial U}{\partial X}$, … are O($\delta$). For a newtonian fluid, at the order δ, we have

$$\sigma_{XX}=\frac{2}{R_e}\frac{\partial U}{\partial X}+\mathrm{O}(\delta^2)=\mathrm{O}(\delta), \tag{A7}$$

$$\sigma_{XY}=\frac{1}{R_e}\left(\frac{\partial V}{\partial X}+\frac{\partial U}{\partial Y}-KU\right)+\mathrm{O}(\delta^2)=\mathrm{O}(1), \tag{A8}$$

$$\sigma_{YY}=\frac{2}{R_e}\frac{\partial V}{\partial Y}=\mathrm{O}(\delta). \tag{A9}$$

Then, at the order δ, the Eqs. (A1), (A2), and (A3) are

$$\frac{\partial U}{\partial X}+\frac{\partial V}{\partial Y}=0, \tag{A10}$$

$$U\frac{\partial U}{\partial X}+V\frac{\partial U}{\partial Y}=-\frac{\partial P}{\partial X}+\frac{\partial \sigma_{XX}}{\partial X}+\frac{\partial}{\partial Y}(1+KY)\sigma_{XY}+K\sigma_{XY}, \tag{A11}$$

$$U\frac{\partial V}{\partial X}-KU^2=-\frac{\partial P}{\partial Y}+\frac{\partial \sigma_{XY}}{\partial X}+\frac{\partial \sigma_{YY}}{\partial Y}, \tag{A12}$$

where the corrresponding Navier-Stokes equations are

$$U\frac{\partial U}{\partial X}+V\frac{\partial U}{\partial Y}=-\frac{\partial P}{\partial X}+\frac{1}{R_e}\left(\frac{\partial^2 U}{\partial X^2}+\frac{\partial}{\partial Y}\left[(1+KY)\frac{\partial U}{\partial Y}\right]\right), \tag{A13}$$

$$U\frac{\partial V}{\partial X}-KU^2=-\frac{\partial P}{\partial Y}+\frac{1}{R_e}\left(\frac{\partial^2 V}{\partial X^2}+\frac{\partial^2 V}{\partial Y^2}\right). \tag{A14}$$

APPENDIX B: LONG-WAVE APPROXIMATION

Let L^* be the influence length of a perturbation in the flow field, i.e., the length of a region where $\frac{\partial v_1}{\partial X}\neq 0$ in the straight or curved parts. Define $L=\frac{L^*}{H}$ and assume that $L\gg 1$.

To analyse the flow on this length scale L, let $\bar{X}=\frac{X}{L}$. Then, the continuity equation implies a scaling of V such as: $\bar{V}=LV$. To focus the analysis on the zones where the flow field is perturbed, we introduce p_1^* defined by

$$p_1^*=p_1-k\int_{Y_c}^{Y}u_0^2\,dY. \tag{B1}$$

The core Eqs. (31) and (32) thus become

$$-u_0\frac{\partial\overline{v_1}}{\partial Y}+\overline{v_1}\frac{du_0}{dY}=-\frac{\partial p_1^*}{\partial\bar{X}}, \tag{B2}$$

$$L^{-2}u_0\frac{\partial\overline{v_1}}{\partial\bar{X}}=-\frac{\partial p_1^*}{\partial Y}. \tag{B3}$$

The analysis of the order of magnitudes in *the boundary layer* of the terms in Eqs. (B2)–(B3) shows that

$$\frac{\partial p_1^*}{\partial\bar{X}}=\mathrm{O}(\varepsilon), \tag{B4}$$

$$\frac{\partial p_1^*}{\partial Y}=\mathrm{O}(\varepsilon^2L^{-2}). \tag{B5}$$

Performing the $\bar{X}$ derivative of Eq. (B3) yields

$$L^{-2}u_0\frac{\partial^2\overline{v_1}}{\partial\bar{X}^2}=-\frac{\partial}{\partial\bar{X}}\left(\frac{\partial p_1^*}{\partial Y}\right). \tag{B6}$$

From Eq. (B6), we deduce that in the core

$$\frac{\partial}{\partial Y}\left(\frac{\partial p_1^*}{\partial\bar{X}}\right)=\mathrm{O}(L^{-2}). \tag{B7}$$

Therefore, using Eq. (B4), we have uniformly

$$\frac{\partial p_1^*}{\partial\bar{X}}=\mathrm{O}(\varepsilon,L^{-2}), \tag{B8}$$

and since both ε and L^{-2} are $\ll 1$, we have everywhere including in the core

$$L\gg 1\Rightarrow\frac{\partial p_1}{\partial\bar{X}}\ll 1. \tag{B9}$$

Therefore, the long-wave approximation implies that in the core, the longitudinal pressure gradient is necessarily «1 and can be neglected in the core, since the inertial terms in the longitudinal Eq. (B2) are O(1), thus leading to the simplified model used in this paper.

The determination of the influence length L, as a function of R_e, can be obtained from the UVA longitudinal momentum equation which can be written, using the previous scaling, as

$$U\frac{\partial U}{\partial \bar{X}}+\bar{V}\frac{\partial U}{\partial Y}=-\frac{\partial p_0}{\partial \bar{X}}-\delta\frac{\partial p_1^*}{\partial \bar{X}}+\frac{L}{R_e}\frac{\partial}{\partial Y}\left[(1+KY)\frac{\partial U}{\partial Y}\right], \tag{B10}$$

where the order of magnitude for the inertial and the viscous terms are, respectively,

$$\mathrm{O}(\varepsilon\delta) \quad \text{and} \quad \mathrm{O}\left(\frac{L\delta}{R_e\varepsilon^2}\right). \tag{B11}$$

In order that inertial and viscous terms in Eq. (B10) to be of the same order, the influence length is, therefore,

$$L=R_e\varepsilon^3. \tag{B12}$$

A particular interesting case is when, see Eq. (B8)

$$L^{-2}=\varepsilon. \tag{B13}$$

Thus at the $\mathrm{O}(\bar{X})$ scale, Eqs. (B12) and (B13) yield

$$L=R_e^{1/7}, \quad \varepsilon=R_e^{-2/7}, \quad \text{and} \quad \frac{\partial p_1^*}{\partial \bar{X}}=\mathrm{O}\left(R_e^{-2/7}\right). \tag{B14}$$

We may say that the present work corresponds to the case where L^{-2} is of the order of ε since our numerical results show that the upstream influence length is of order $Re^{1/7}$, therefore the long-wave approximation is justified.

APPENDIX C: CURVATURE DISCONTINUITIES TREATMENT

In order to numerically treat curvature discontinuities, we use the following change of variables:

$$v_1^*=v_1-u_0\int_{-\infty}^{X}k(\xi)d\xi, \tag{C1}$$

where $-\infty$ represents the inlet of the upstream straight channel.

Therefore, Eq. (40) for v_1 can be written

$$v_1^*=-u_0A^{*\prime}(X) \quad \text{where} \quad A^{*\prime}(X)=A'(X)+\int_{-\infty}^{X}k(\xi)d\xi. \tag{C2}$$

Similarly, Eq. (41) becomes

$$-u_0^2A^{*\prime\prime}(X)=-\frac{\partial p_1}{\partial Y}, \tag{C3}$$

Eq. (42) becomes

$$p_1=A^{*\prime\prime}\int_{Y_c}^{Y}u_0^2(Y')\,\mathrm{d}Y'+B(X), \tag{C4}$$

and Eq. (43) becomes

$$\frac{\partial P_1}{\partial X}=\frac{\mathrm{d}p_0}{\mathrm{d}X}+\delta A^{*\prime\prime\prime}\int_{Y_c}^{Y}u_0^2(Y')\,\mathrm{d}Y'+\delta B'(X). \tag{C5}$$

Thus, in the system to solve, neither k or k' appears, but only $\int_{-\infty}^{X}k(\xi)d\xi$.

[1]W. R. Dean, "Note on the motion of fluid in a curved pipe," Philos. Magn. **20**, 208 (1927).
[2]W. R. Dean, "Fluid motion in a curved channel," Proc. R. Soc. London, Ser. A **121**, 402 (1928).
[3]S. A. Berger, L. Talbot, and L. S. Yao, "Flow in curved pipes," Annu. Rev. Fluid Mech. **15**, 461 (1983).
[4]T. J. Pedley, *The Fluid Mechanics of Large Blood Vessels* (Cambridge University Press, New York, 1980).
[5]H. Ito, "Flow in curved pipes," JSME Int. J. **30**(262), 543 (1987).
[6]A. J. Ward-Smith, *Pressure Losses in Ducted Flows* (Butterworths, London, 1971).
[7]A. J. Ward-Smith, *Internal Fluid Flow: The Fluid Dynamics of Flow in Pipes and Ducts* (Clarendon, Oxford, 1980).
[8]A. C. Hurd and A. R. Peters, "Analysis of flow separation in a confined two-dimensional channel," J. Basic Eng. **92**(4), 908 (1970).
[9]B. Snyder and C. Lovely, "A computational study of developing 2-d laminar-flow in curved channels," Phys. Fluids A: Fluid Dyn. **2**(10), 1808 (1990).
[10]F. T. Smith, "On the high Reynolds number theory of laminar flows," IMA J. Appl. Math. **28**(3), 207 (1982).
[11]I. J. Sobey, *Introduction to Interactive Boundary Layer Theory* (Oxford University Press, New York, 2000).
[12]J. Mauss and J. Cousteix, "Uniformaly valid approximations for singular perturbation problems and maching principle," C. R. Méc. **330**, 697 (2002).
[13]J. Cousteix and J. Mauss, *Asymptotic Analysis and Boundary Layers*, Scientific Computation, Vol. XVIII (Springer, Berlin, Heidelberg, 2007).
[14]J. Cousteix and J. Mauss, "Approximations of navier-stokes equations at high Reynolds number past a solid wall," J. Comput. Appl. Math. **166**(1), 101 (2004).
[15]P. Cathalifaud, J. Mauss, and J. Cousteix, "Nonlinear aspects of high Reynolds number channel flow," Eur. J. Mech. B/Fluids **29**(4), 295 (2010).
[16]J. Cousteix and J. Mauss, "Interactive boundary layer models for channel flow," Eur. J. Mech. B/Fluids **28**, 72 (2009).
[17]H. Ito, "Pressure losses in smooth pipe bends," Trans. ASME, Ser. D **82**(1), 131 (1960).
[18]F. T. Smith, "Upstream interactions in channel flows," J. Fluid Mech. **79**, 631 (1977).
[19]K. Stewartson and P. G. Williams, "Self induced separation," Proc. R. Soc. London, Ser. A **312**, 181 (1969).